Accepted Manuscript

Interfacial properties of Cu/Ni/Mg_2Si joints prepared in one step by the spark plasma sintering method

Renyao Yang, Shaoping Chen, Wenhao Fan, Xiufeng Gao, Yang Long, Wenxian Wang, Zuhair A. Munir

PII: S0925-8388(17)30509-1

DOI: 10.1016/j.jallcom.2017.02.082

Reference: JALCOM 40810

To appear in: *Journal of Alloys and Compounds*

Received Date: 8 September 2016

Revised Date: 25 January 2017

Accepted Date: 9 February 2017

Please cite this article as: R. Yang, S. Chen, W. Fan, X. Gao, Y. Long, W. Wang, Z.A. Munir, Interfacial properties of Cu/Ni/Mg_2Si joints prepared in one step by the spark plasma sintering method, *Journal of Alloys and Compounds* (2017), doi: 10.1016/j.jallcom.2017.02.082.

Interfacial Properties of Cu/Ni/Mg_2Si Joints Prepared in One Step by the Spark Plasma Sintering Method

Renyao Yang [1], Shaoping Chen [1,2], Wenhao Fan [3], Xiufeng Gao[1], Yang Long [1], Wenxian Wang [2], and Zuhair A. Munir[4]

(1. Key Laboratory of Interface Science and Engineering in Advanced Materials, Ministry of Education, Taiyuan University of Technology, Taiyuan 030024, China. 2. College of Materials Science and Engineering, Taiyuan University of Technology, Taiyuan 030024, China. 3. College of Physics and Optoelectronics, Taiyuan University of Technology, Taiyuan 030024, China. 4. Department of Material Science and Engineering, University of California, Davis, CA 95616, USA.)

Abstract

Cu/Ni/Mg_2Si thermoelectric bonded joints were prepared in one step by the spark plasma sintering (SPS) method using Mg and Si powders to form Mg_2Si. The microstructure and elemental distribution across the interfaces were determined, and the formation of new phases at the interface was investigated and related to joint properties, including shear strength and contact resistance. Joint formation was accompanied by the formation of two ternary Mg-Si-Ni layers, an η-layer with Ni_2Si as a precipitate next to Ni, and an ω-layer next to Mg_2Si. The formation and characteristics of these layers played a major role in determining the shear strength and contact resistance. It was determined that a reactive sintering temperatures in the range 1023-1053K with a 15-20 min hold time provided the best properties. The maximum shear strength of the joints obtained is 26MPa for samples sintered at 1023K. For these samples the contact resistance was 1.44 mΩ•cm^2; the minimum value of 1.28mΩ•cm^2 was measured for samples sintered at 1073K. Long-term thermal stability of joints was also investigated.

Keywords: Thermoelectric Materials; SPS; Magnesium Silicide; Shear Strength; Contact Resistance

1. Introduction

The predicted increase in energy demands globally **[1]** and the concern about environmental degradation have prompted efforts to develop clean and sustainable energy sources **[2]**. In this regard, efforts to identify and develop new energy sources and to utilize waste heat have shown significant potential benefits. Thermoelectric materials, as functional materials that can convert thermal energy directly into electric energy, have a wide potential application in generators and coolers. The added advantages of such devices are that they contain no moving parts, are lightweight, small, and nearly vibration-free **[1-3]**.

N-type magnesium silicide (Mg_2Si) is a candidate thermoelectric (TE) material operating in the temperature range of 600 to 900 K. It is nontoxic, environmentally benign, and is relatively abundant in the earth's crust **[4-6]**. For an ideal Mg_2Si-based TE device with a high-output power, a stable and effective connection between the thermoelectric material and the electrode is necessary. Generally, the traditional electrode is made of low-resistivity metals that can bond well with the TE material. Metals such as copper, nickel, silver and their alloys are potential candidates **[7-8]**. Because of its relatively low price, high electrical and thermal conductivity and a similar coefficient of thermal expansion (CTE) to that of Mg_2Si, copper is commonly selected as an electrode with one or two metal inter-layers **[9-10]**. The high cost of silver limits its applications as an electrode or barrier material. And for the case of Ni, complex new phases that may form at the Ni/Mg_2Si interface complicate the relationship between processing and the contact resistance of the product **[8]**. To enhance the output power and reduce the contact resistance, efforts have been made to develop appropriate electrode materials for magnesium silicide **[11-13]**. Transition metal silicides, such as $CoSi_2$, $CrSi_2$, $TiSi_2$, and NiSi have been utilized as electrode materials for the n-type Mg_2Si. A maximum output power of 153 mW was reported with $CoSi_2$ as the electrode, representing an increase of 27% relative to the use of nickel at 600K **[12]**.

Tohei et al. **[9]** utilized aluminum instead of a silver-alloy braze to bond Mg_2Si to Ni and reported a shear strength of 19 MPa. Ferrario et al. **[10]** investigated n-type Mg_2Si samples on which metal contacts (Au, Cu, Ni, Al, and Ti) were deposited by DC magnetron sputtering. De Boor et al. **[8]** have prepared Sb-doped Mg_2Si samples with Ni electrodes using a one-step sintering technique and observed an intermediate layer which consisted of different ternary phases of Mg/Si/Ni and $Si_{12}Ni_{31,}$ which showed good adhesion to both the Ni electrode and the Mg_2Si.

To ensure stable and long-life performance, it is important to determine the formation (amount, morphology) and role (high-temperature evolution in service) of new phases at the interfaces of dissimilar materials. Despite the abundance of reports on the bonding between nickel (and similar electrode materials) and magnesium silicide by different methods, there is an apparent lack of studies on the thermal stability of the interface, and also on the formation process of the new phases and their effect on joint strength and contact resistance. In this study, Ni was selected as the diffusion barrier and buffer layer between a Cu electrode and Mg_2Si. A Cu/Ni/Mg_2Si ensemble was fabricated by a one-step spark plasma sintering (SPS) process. The morphology, distribution, composition of the new phases is investigated, as well as the. shear strength, thermal stability, and contact resistance.

2. Experimental Materials and Methods

The starting materials used in this study were powders of magnesium (≤50μm, 99.5% pure) and silicon (≤45μm, 99.99% pure), a disk-shaped copper substrate (Φ20×0.3mm, 99.5% pure), and a nickel foil (Φ20×0.05mm, 99.5% pure). All materials were obtained from Aladdin Co. in Shanghai. The goal was to form a symmetric structure of Cu/Ni/Mg_2Si/Ni/Cu in order to simulate the real heat and current flow distribution. Powder mixture of magnesium and silicon was weighed in the stoichiometric ratio of 2:1 and then milled in a high-speed ball mill (QM-3B) for 30 min with a ball-to-powder mass ratio of 10:1. A fixed amount of the mixed powders, 2 g, was then cold-pressed on top of a Ni/Cu couple and then covered by the other Cu/Ni couple to form a

structure of Cu/Ni/Mg_2Si/Ni/Cu inside a graphite die. The pressed powder had a relative density about 60%. The ensemble was placed inside a graphite die with a 20.5 mm diameter. Two graphite plungers were added to the two ends of the die; all handling was done under an inert gas atmosphere. Reaction synthesis and bonding were carried out in a spark plasma sintering apparatus (SPS, Dr. Sinter Lab 211Lx) under a vacuum of 6 Pa. Details of the SPS method and its advantages are provided elsewhere in a feature article [**14**].

Samples were sintered at different temperatures (923, 973, 1023, and 1073K) for 5-30 min at a pressure of 50 MPa. The temperature of the samples was measured by a W-5%Re-W-26%Re thermocouple (OMEGA, diameter 0.3 mm), which was placed inside a hole drilled in the graphite die. The tip of the thermocouple was about 2 mm from the sample. The microstructure and phase composition of the prepared samples were determined by scanning electron microscopy (SEM, JSMJEOL 6390) and energy dispersive spectroscopy (EDS, HKL). Contact resistance was measured by the four-point probe method **[15]** on the sample arrangement shown schematically in **Fig.1 (a).** More details on this method are provided elsewhere **[16]**. The voltage measured across the inner probes is used to calculate the Mg_2Si material conductivity, while the voltage across the outer probes provided information on the contact resistance at the Ni/Mg_2Si interface. The specimens used for this evaluation were 4×4×δ mm in dimension, with δ being the thickness of the sample, typically 4-5 mm. The shear strength of the resulting joints was measured by a microcomputer-controlled electronic universal testing machine (DNS200) with a head movement rate of 1mm.min^{-1}. The specimens used for this evaluation were 7×7×δ mm in dimension (δ = 4-5 mm). A schematic of this measurement is shown in **Fig. 1 (b)**. For thermal stability investigations, samples were sealed in evacuated silica tubes and annealed at 723K for 100, 300, and 600 h.

3. Results and Discussion

3.1 Properties of Joints

Although there are four interfaces in the symmetric ensemble of Cu/Ni/Mg_2Si/Ni/Cu, we

focused on the two Ni/Mg_2Si interfaces, ignoring the Cu/Ni interfaces. The justification for this is based on two reasons: first, observations in a previous study **[17]** showed that the direction of the direct current had no effect on the elemental diffusion across the interfaces in this symmetric ensemble. Second, Cu and Ni form a solid solution over the entire compositional limits, with no intermetallic compounds. Additionally, the Ni foil was sufficiently thick so that Cu atoms are not likely to diffuse through to the Ni/Mg_2Si interface, as will be shown later.

The temperature dependence of the shear strength and the interface contact resistance of Cu/Ni/Mg_2Si/Ni/Cu joints prepared at different temperatures (923, 973, 1023 and 1073K) with a holding time of 15 min are shown in **Fig.1(c)**. The figure shows a strong dependence of both parameters on the sintering temperature. With an increase in sintering temperature, the shear strength increased to a maximum at 1023K and then decreased, while the contact resistance decreased continuously to a value of 1.28 mΩ•cm^2 at 1073K. These observations indicate that sintering in the temperature range between 1023 and 1053K appears to provide the best properties.

To explore the relationship between sintering temperature and the resulting properties, the microstructure and phase composition of the Ni/Mg_2Si interface of samples sintered at different temperatures, excluding 923K, were investigated. Samples sintered at 923K had unattractive properties and thus are not further considered. **Fig.2 (a), (b), and (c)** show SEM images of samples sintered for 15 min at 973, 1023, and 1073K, respectively. The figures show two intermetallic layers that formed at the Ni/Mg_2Si interface. EDS analyses of the regions indicated by numbers in **Fig.2 (a)** are listed in **Table1**.The results show that region 1 is pure Ni and region 4 is Mg_2Si. Region 2 contains two phases, a continuous phase (dark gray), determined as $Mg_6Si_7Ni_{16}$ (referred to as the η-phase) and a precipitate (lighter gray), determined to be Ni_2Si. Region 3 is determined as an Mg, Si, Ni ternary, designated by Song and Varin **[18]** as the ω phase. The present results are in agreement with the findings of these authors who investigated interactions in the Ni-Si-Mg ternary diagram. We have used their phase designation in this work.

In **Fig.2 (a)** the thickness of the entire diffusion layer of the sample sintered at 973K is roughly 5μm, in which the thickness of the η layer is about 4μm and the thickness of the ω-layer is about 1μm. For samples sintered at 1023K, **Fig.2 (b)**, the total thickness of the diffusion layer is nearly 8μm. The increase in total thickness is due primarily to an increase in the η-layer; the ω-layer appears to have not changed. Furthermore, the Ni_2Si precipitate in the η-layer increased, with an associated change in its morphology from generally isolated particles to a more continuous uniform distribution. With the further increase in temperature to 1073K, **Fig.2 (c)**, the thickness of the η-layer showed no increase but the Ni_2Si precipitates grew considerably, forming a continuous network and becoming a major part of the η-layer. At this temperature, the ω-layer appears to have nearly disappeared. The total thickness of the diffusion layer is approximately unchanged as the sintering temperature increased from 1023 to 1073K.

Two possible explanations for the thickness evolution in the diffusion layer with temperature may be considered: either the ω-phase becomes thermodynamically less stable at higher temperature (1073K), or that the substantial growth of the precipitate Ni_2Si has been at the expense of the ω-phase. By comparing **Fig.2 (a)** and **Fig.2 (b)**, we observe that the thickness of the ω layer is nearly the same, but the amount of the precipitate Ni_2Si at 1023K, **Fig.2 (b)**, is significantly higher than that seen at lower temperature, **Fig.2 (a)**. Thus, it is reasonable to discount the second possibility. And, as indicated above, with a temperature increase from 973K to 1023K, the thickness of the η-layer increased while that of the ω-layer shows no significant change. This observation indicates that the growth of the η-phase is not due to the consumption of the ω-phase within this temperature range. We believe the growth of the η-phase and the increase in the relative amount of the Ni_2Si phase is due to an increase in the diffusion of Ni through the η-layer and the Si through the ω-layer. We suggest that at the highest temperature, 1073K, the diffusion of Ni exceeds that of Si through the ω-layer with the result that the ω-phase is now being consumed by the formation of the precipitate Ni_2Si. The implication of this suggestion is that the Ni_2Si phase is thermodynamically more stable

than the ω-phase at this temperature. We are not cognizant of any information on the relative stabilities of these phases at different temperatures.

While the presence of dispersed Ni_2Si is expected to contribute to higher strength, its continuous net-shaped morphology can contribute adversely due to its brittleness. This is also supported by preliminary shear fracture observations we made of samples sintered at 1073K. The fracture occurred at the η/ω interface and expanded into the η-layer.

Based on the above analysis, we suggest that the thickness of the ω-layer plays a role in determining the strength of the joint: the wider the ω-layer, the stronger the joint. At the highest sintering temperature, 1073K, the ω-layer is small and is associated with a lower shear strength, as seen in **Fig.1 (c)**.

The resistance measured by the outer probe, R_{tot}, is given by

$$R_{tot} = 2R_{Cu} + 2R_{Ni} + 2R_c + 2R_{Ni/Cu} + R_{Mg2Si} \quad (1)$$

Where R_{Cu} and R_{Ni} refer to the resistance of the copper and nickel layers, respectively, R_c is the contact resistance of the interface between the Ni and Mg_2Si, $R_{Ni/Cu}$ is the resistance of the interface between the Cu and Ni layers, and R_{Mg2Si} is of the resistance of the Mg_2Si layer. Because of the high conductivities of Cu and Ni and the Cu/Ni interfaces, Eq (1) can be approximated by

$$R_{tot} \approx 2R_c + R_{Mg2Si} \quad (2)$$

R_{Mg2Si} is calculated from conductivity measurement with the inner probe of **Fig.1 (a),** and with the formation of the new phases between the Ni and Mg_2Si layers on both sides of Mg_2Si, $2R_c \approx 2(R_\eta + R_\omega)$ and thus,

$$R_c \approx R_\eta + R_\omega \quad (3)$$

By comparing the microstructure and properties of samples prepared at 973K, **Fig.2 (a)**, and at 1023K, **Fig.2 (b)**, we observe that the total thickness of the diffusion layer had increased from about 5 to about 8μm. This was predominantly due to an increase of the η-layer since the ω-layer was nearly unchanged. Associated with this change is a decrease in the resistance, from 20 to 7.5 mΩ,

as seen in **Fig.1 (c)**. This observation indicates that the main factor that affects the contact resistance is the nature (microstructure) of the η-layer and not its thickness. As seen in **Fig.2**, the η-layer includes Ni_2Si as a second phase. Thus, the decrease in resistance is associated with a change in the amount and microstructure of the Ni_2Si in the η-layer. As the temperature increased, the Ni_2Si phase increased and became more continuous in morphology. The effect of morphology is seen when comparing the microstructures obtained at 1023K and 1073K, **Figs. 2 (b)** and **2 (c)**, respectively. While the thickness of the η-layer did not show a significant change, the resistance decreased by a small amount, which is attributed to the increase in the relative amount of the Ni_2Si phase and the change in its morphology. The implication of the above is that the amount and microstructure of Ni_2Si in the η-layer contribute to a lower contact resistance at the Ni/Mg_2Si interface. The resistivity of nickel silicide is reported to be less than that of Mg_2Si **[12].**

To provide justification for the suggested correlation and to further investigate the formation process of Ni_2Si, experiments on $Cu/Ni/Mg_2Si/Ni/Cu$ joints were carried out at 1023K with different holding times: 5, 10, 15, 20 and 30 min. The results of these experiments are shown in **Fig. 3** as shear strength and interface contact resistance dependence on sintering time at this temperature. With an increase in sintering time, the shear strength increased linearly while the contact resistance decreased as sintering time was increased from 5 to 15 min and then increased as the sintering time increased to 30 min. These results indicate that a 15-20 min sintering time would provide the best results for contact resistance.

The microstructures of the diffusion layers resulting from holding the samples at 1023K for 5, 15, and 30 min are shown in **Figs. 4 (a)**, **2 (b)** and **4 (b)**, respectively. The figures show the presence of the two intermetallic layers: η-layer, with the Ni_2Si precipitate, and the ω-layer. The thickness of the former is greater than that of the latter, as indicated above. With an increase in sintering time, little change in the thickness of the η-layer was observed, with a typical value of about 6 μm, but the amount of the precipitate Ni_2Si increased. However, while the η-layer remained nearly constant,

the thickness of the ω-phase increased markedly, from about 0.5 to 1.0 to 2.0 μm for a 5, 15, and 30 min hold, respectively. This observation indicates that, at this temperature (1023K), the formation of the Ni_2Si phase is not at the expense of the ω-phase, implying that the latter is thermodynamically stable relative to Ni_2Si at this temperature. These results further show that the increase in thickness of the ω-layer with holding time is associated with an increase in the shear strength with holding time, as seen in **Fig. 3**.

The observations discussed above suggest that the contact resistance is decreased by the formation and microstructure of the Ni_2Si phase and is increased by the formation of the ω-layer. The shear strength on the other hand is enhanced by the formation of the ω-layer.

Several studies have been reported in which contact resistance was determined for pure and alloyed Mg_2Si. Nakamura et al. **[19]** used a commercially prepared Mg_2Si powders which were then milled and sintered and obtained a contact resistance (with Ni electrodes) of ≈ 0.5 $m\Omega.cm^2$, a value in reasonable agreement with that obtained in this study, 1.28 $m\Omega.cm^2$. Sakamoto et al. **[12]**, using commercial Mg_2Si obtained a contact resistance of 0.95 $m\Omega.cm^2$ on samples with Ni electrodes. However, in studies using alloyed Mg_2Si, the reported contact resistance is significantly lower: 4.4 $\mu\Omega\bullet cm^2$ reported by de Boor et al. for Sb-doped Mg_2Si **[8]** and 5.5 $\mu\Omega.cm^2$ reported by Thimont et al. for Bi-doped Mg_2Si **[15]**. In contrast to the previous studies identified here, the synthesis of Mg_2Si (from elemental powders) in the present study was done simultaneously with the process of bonding to the Ni and the electrodes.

3.2 Effect of Long-Term Annealing on the Performance of Joints

To investigate the effect of long-term thermal annealing on the stability, shear strength, and contact resistance of prepared joints, samples which had been sintered at various temperatures were annealed for up to 600 h at 723K. **Fig.5 (a)** shows the effect of annealing time on the shear strength of samples sintered at various temperatures, and **Fig.5 (b)** shows the corresponding effect on contact resistance. In both cases the data for the samples prior to annealing are also included. The shear

strength of joints increased after annealing for 100 h then decreased with longer annealing time; the maximum value of the shear strength was for samples sintered at 1023K. The trend with sintering temperature is analogous to that for samples that had not been annealed. The microstructures of samples sintered at 1023K and annealed at 723K for 100, 300 and 600 h are shown in **Figs. 6 (a)**, **(b)**, and **(c)**, respectively. A comparison between these microstructures and those of samples before annealing, **Fig.2 (b)**, shows that the thickness of the ω-layer had increased from 1μm to 3μm after annealing for 100h, providing support to the conclusion that a well-developed ω-layer enhances shear strength. However, it can be seen that longer annealing time results in the formation of cracks within the ω-layer and near the boundary between this layer and the η-layer, as can be seen from **Figs.6 (b)** and **(c).**

Figs.7 (a) and **(b)** show a SEM image of a fracture surface and the back-scattered diffraction (BSD) image of the surface, respectively. The BSD image indicates the fracture surface is nearly all composed of Mg_2Si with small amounts of phases approximating the compositions of the η and ω phases. These results imply that fracture occurred within the Mg_2Si layer or near to the Mg_2Si/η interface. However, when the annealing time was increased to higher values (300 and 600 h), crack formation was observed, as indicated above. The formation of cracks with longer annealing time may be due to a relaxation time needed to accommodate differences in the coefficients of the thermal expansion (CTE) between the ω-and η-layers. Or possibly that the transport of Si atoms through the ω-layer is slower relative to that in the η-layer, a circumstance that would lead to vacancy formation near the η-layer/ω-layer interface. The presence of cracks is believed to be the cause of the observed decrease in the shear strength, **Fig.5 (a)**.

Fig.5 (b) shows the effect of long-term annealing on the contact resistance of samples sintered at different temperatures. In all cases the resistance increased with annealing time. The increase is believed to be due to the growth of the ω-layer, and also due to the presence of cracks.

3. Conclusions

Joints of the thermoelectric ensemble Cu/Ni/Mg_2Si/Ni/Cu were prepared and bonded in one step by the SPS method using powders of Mg and Si to form Mg_2Si. Joints were made at different temperatures and for different holding times. Two phases formed at the interface between Ni and Mg_2Si: the η and ω ternary phases. The former contained Ni_2Si as precipitate. Microstructural observations showed that the contact resistance is decreased by the growth of the η-layer with its Ni_2Si precipitate, and increased by the growth of the ω-layer. The growth of the ω-layer enhanced the shear strength. Samples sintered for 15 min at 1023K provided the optimum shear strength and contact resistance. An optimum shear strength of about 20 MPa was achieved for samples sintered at 1023K for 15 min, and a concomitant contact resistance of 1.44 $m\Omega.cm^2$.

The stability of the joints was investigated by long-term annealing at 723K for a maximum of 600 h for samples sintered at various temperatures. Annealing of samples sintered at 1023K for 100 h resulted in an increase of the shear strength to 23 MPa and an increase in the contact resistance to 3.7 $m\Omega.cm^2$.

Acknowledgments

This research was supported by the National Science Foundation of China through Grant No. 51101111, 51405328 and the Shanxi Province Science Foundation through Grant No. 201601D011033. Additional support from our group members is gratefully acknowledged.

Reference

[1] L. E. Bell. Cooling, heating, generating power, and recovering waste heat with thermoelectric systems. Science, 2008, 321(5895): 1457

[2] F. J. Disalvo. Thermoelectric cooling and power generation. Science, 1999, 285(5428): 703-706.

[3] W. Liu, Q. Jie, H.S. Kim, and Z. F. Ren. Current progress and future challenges in thermoelectric power generation: From materials to devices. Acta. Mater. 2015, 87:357.

[4] W. Liu, H. Wang, L. Wang, X. W. Wang, G. Joshi, G. Chen, and Z. F. Ren. Understanding of the contact of nanostructured thermoelectric n-type $Bi_2Te_{2.7}Se_{0.3}$ legs for power generation applications. J. Mater. Chem. 2013, 1(42):13093.

[5] X. Liu, T. Zhu, H. Wang, L. P. Hu, H. H. Xie, G. Y. Jiang, G. Jeffrey Snyder, and X. B. Zhao. Low Electron Scattering Potentials in High Performance $Mg_2Si_{0.4}Sn_{0.55}$ Based Thermoelectric Solid Solutions with Band Convergence. Adv. Energy. Mater. 2013, 3(9):1238.

[6] P. Gao, X. Lu, I. Berkun, R. D. Schmidt, E. D. Case, and T. P. Hogan. Reduced lattice thermal conductivity in Bi-doped $Mg_2Si_{0.4}Sn_{0.6}$. Appl. Phys. Lett. 2014, 105(20), 202104.

[7] W. Liu, Q. Zhang, K. Yin, H. C, X. Y. Zhou, X. F. Tang, and C. Uher. High figure of merit and thermoelectric properties of Bi-doped $Mg_2Si_{0.4}Sn_{0.6}$, solid solutions. J. Solid State Chem. 2013, 203(7):333-339.

[8] J. de Boor, C. Gloanec, H. Kolb, R. Sottong, P. Ziolkowski, and E. Müller. Fabrication and characterization of nickel contacts for magnesium silicide based thermoelectric generators. J. Alloy. Comp. 2015, 7:348-353.

[9] T. Tohei, S. Fujiwara, T. Jinushi, and Z. Ishijima. Bondability of Mg_2Si element to Ni electrode using Al for thermoelectric modules. Mater. Sci. Eng. 2014.

[10] A.Ferrario, S. Battiston, S. Boldrini, T. Sakamoto, E. Miorin, A. Famengo, A. Miozzo, S.

Fiameni, T. Iida, and M. Fabrizio. Mechanical and Electrical Characterization of Low-resistivity Contact Materials for Mg_2Si. Mater. Today. Proceed. 2015, 2(2):573-582.

[11] T. Sakamoto, T. Iida, N. Fukushima, Y. Honda, M. Tada, Y. Taguchi, Y. Mito, H. Taguchi, and Y. Takanashi. Thermoelectric properties and power generation characteristics of sintered undoped n-type Mg_2Si. Thin Solid Films. 2011, 519(24):8528-8531.

[12] T. Sakamoto, T. Iida, Y. Honda, M. Tada, T. Sekiguchi, K. Nishio, Y. Kogo, and Y. Takanashi. The Use of Transition Metal Silicides to Reduce the Contact Resistance Between the Electrode and Sintered n -Type Mg_2Si. J. Electron. Mater. 2012, 41(6):1805-1810.

[13] T. Nemoto, T. Iida, J. Sato, T. Sakamoto, N. Hirayama, T. Nakajima, and Y. Takanashi. Development of an Mg_2Si Unileg Thermoelectric Module Using Durable Sb-Doped Mg_2Si Legs. J. Electron. Mater. 2013, 42(7):2192-2197.

[14] Z. A. Munir, D. V. Quach, and M. Ohyanagi. Electric Current Activation of Sintering: A Review of the Pulsed Electric Current Sintering Process, *J. Amer. Ceram. Soc.*, **94**, 1-19 (2011).

[15] Y. Thimont, Q. Lognoné, C. Goupil, F. Gascoin, and E. Guilmeau. Contact Resistance Determination for Thermoelectric Leg. J. Electron. Mater. 2014, 43(6):2023.

[16] S. Bai, F. Li, T. Wu, X. Yin, X. Shi, and L. Chen. Interface characterization of Cu–Mo coating deposited on Ti–Al alloys by arc spraying. Funct. Mater. Lett., 8, 1550048 (2015).

[17] S. P. Chen. Diffusion Bonding Mechanism and Properties of the Joints Between Gradient Cermets and Metals Bonded by the FAPAS process. Dissertation, Taiyuan University of Technology. China, 2011.

[18] Y. K. Song and R. A. Varin. Phase equilibria and intermetallic phases in the Ni-Si-Mg ternary system. Metall. Mater. Trans. A. 2000, 32(1): 5.

[19] S. Nakamura, Y. Mori, and K. Takarabe. Analysis of the microstructure of Mg_2Si thermoelectric devices, J. Electron. Mater. 2014, 43: 2174.

Table 1. Results of EDS analysis of the five numbered regions in Fig.2 (a)

Region No.	Ni/at%	Mg/at%	Si/at%
1	99.7	0.2	0.1
2	51.13	19.25	29.62
3	32.62	28.09	39.30
4	1.0	73.2	25.8
5	60.54	5.65	33.82

Figure Captions:

Fig. 1. (a). Schematic configuration of contact resistance measurement.
（b）Schematic diagram for sample shear strength measurement: dimensions are 7 mm×7 mm.
（c）Shear strength and contact resistance of Cu/Ni/Mg_2Si joints formed after 15 min sintering at different temperatures.

Fig. 2. SEM images of Ni/Mg_2Si interfaces after sintering for 15 min at different temperatures: (a) 973K, (b) 1023K, (c) 1073K. From left to right the layers are: pure nickel, η-layer which is composed of the η-phase (dark gray) and precipitates of Ni_2Si (light gray), ω phase, and Mg_2Si.

Fig. 3. Effect of sintering time on the shear strength and contact resistance of Cu/Ni/Mg_2Si joints formed at 1023K.

Fig. 4. Microstructure of Cu/Ni/Mg_2Si interfaces formed at 1023K with different holding times: (a) 5 min, (b) 30 min.

Fig. 5 Effect of annealing time at 723K on: (a) shear strength and (b) contact resistance of Cu/Ni/Mg_2Si joints sintered at different temperatures for 15 min.

Fig. 6. Microstructure of the Cu/Ni/Mg_2Si interface sintered at 1023K after annealing at 723K for (a) 100 h, (b) 300 h, (c) 600 h.

Fig. 7 (a) SEM image and (b) BSD image of a fracture surface of a sample sintered at 1023K for 30 min and annealed at 723K for 100 h.

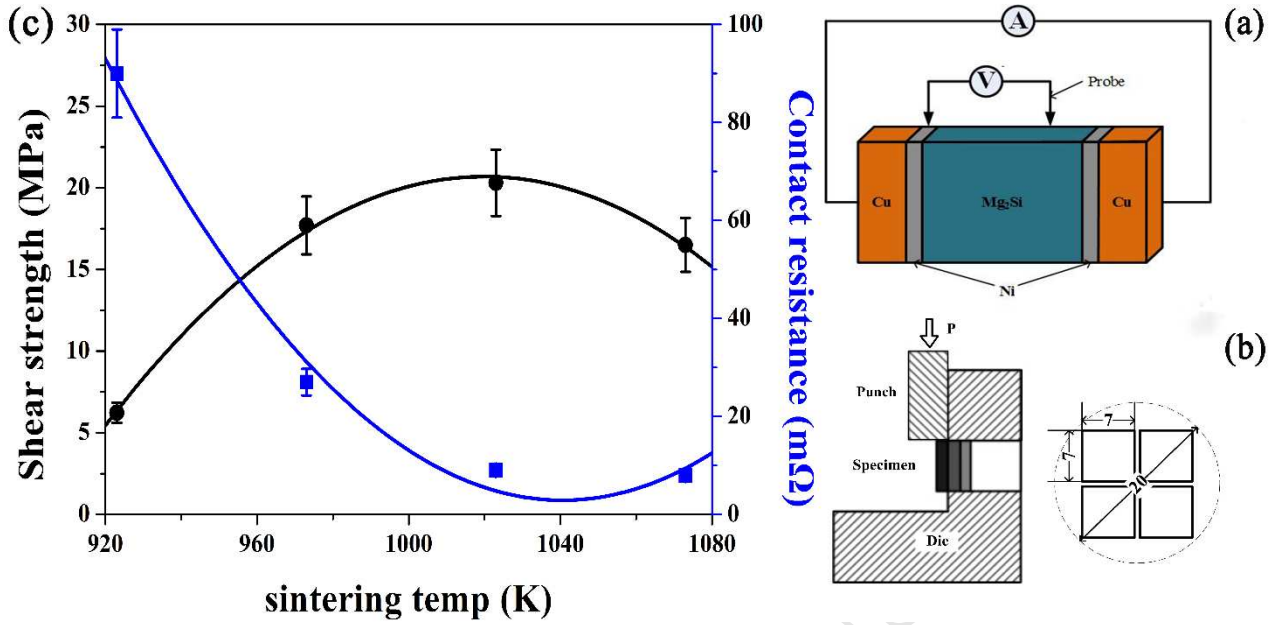

Fig. 1.（a）Schematic configuration of contact resistance measurement.（b）Schematic diagram for sample shear strength measurement: dimensions are 7 mm×7 mm. （c）Shear strength and contact resistance of Cu/Ni/Mg_2Si joints formed after 15 min at different temperatures.

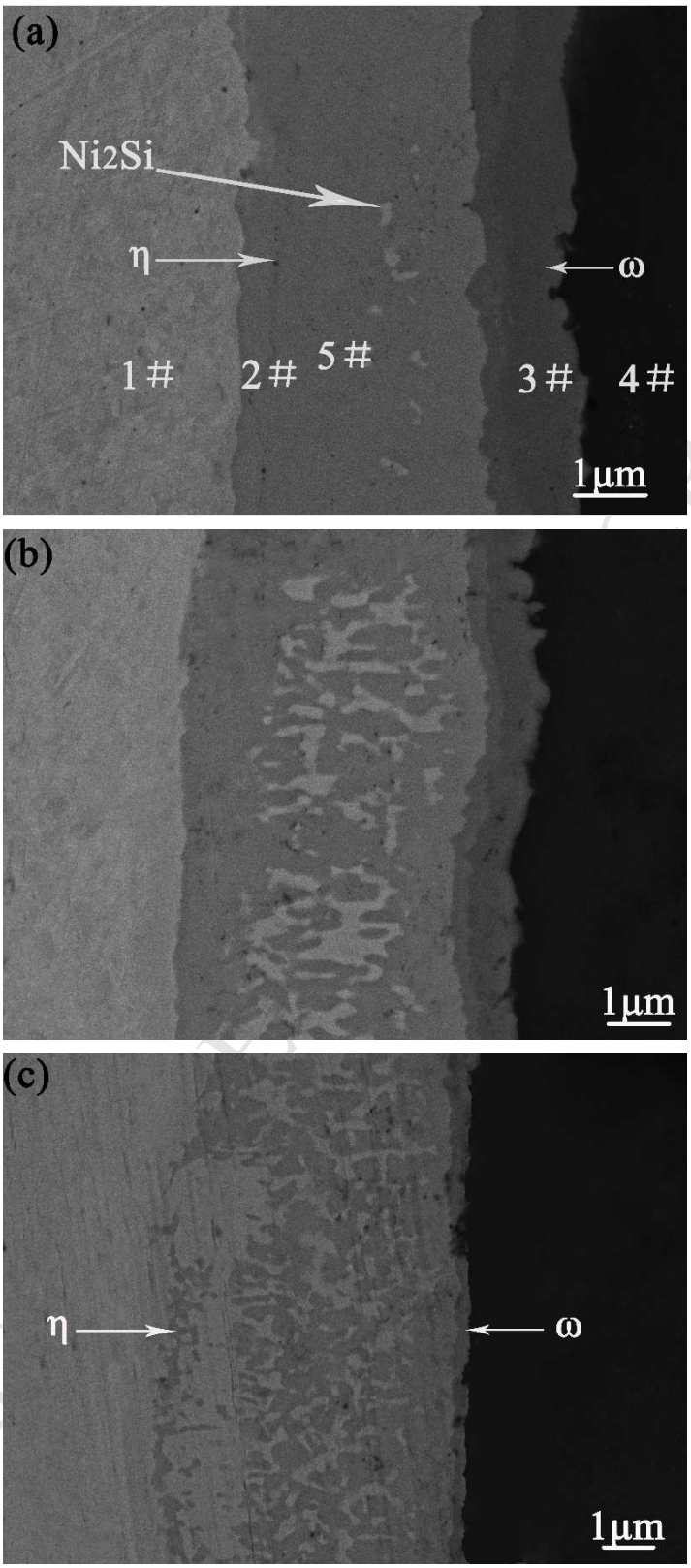

Fig. 2. SEM images of Ni/Mg_2Si interfaces after sintering for 15 min at different temperatures: (a) 973K, (b) 1023K, (c) 1073K. From left to right the layers are: pure nickel, η-layer which is composed of the η-phase (darker gray) and precipitates of Ni_2Si (lighter gray), ω phase, and Mg_2Si

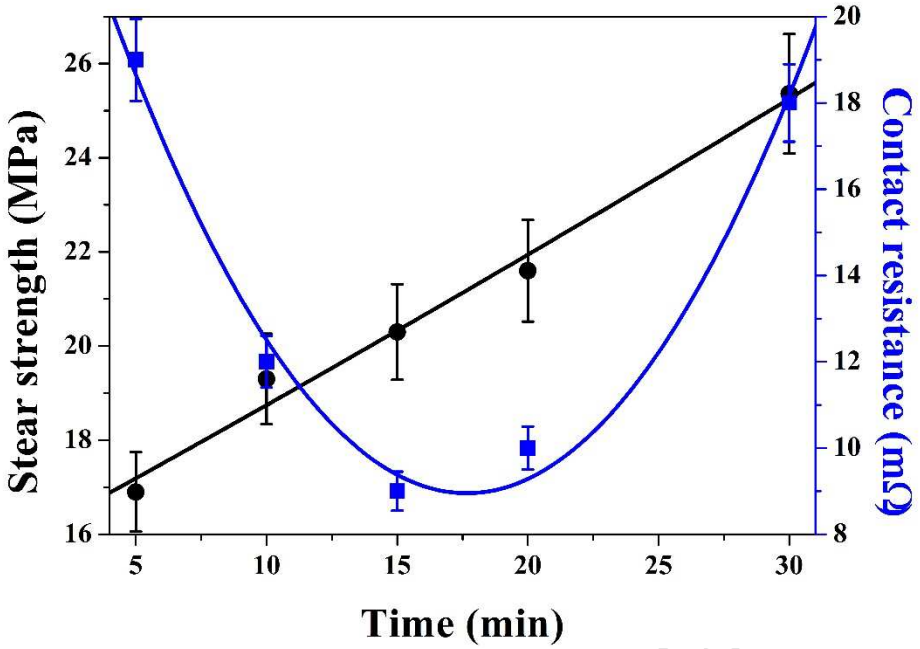

Fig. 3. Effect of sintering time on the shear strength and contact resistance of Cu/Ni/Mg_2Si joints formed at 1023K.

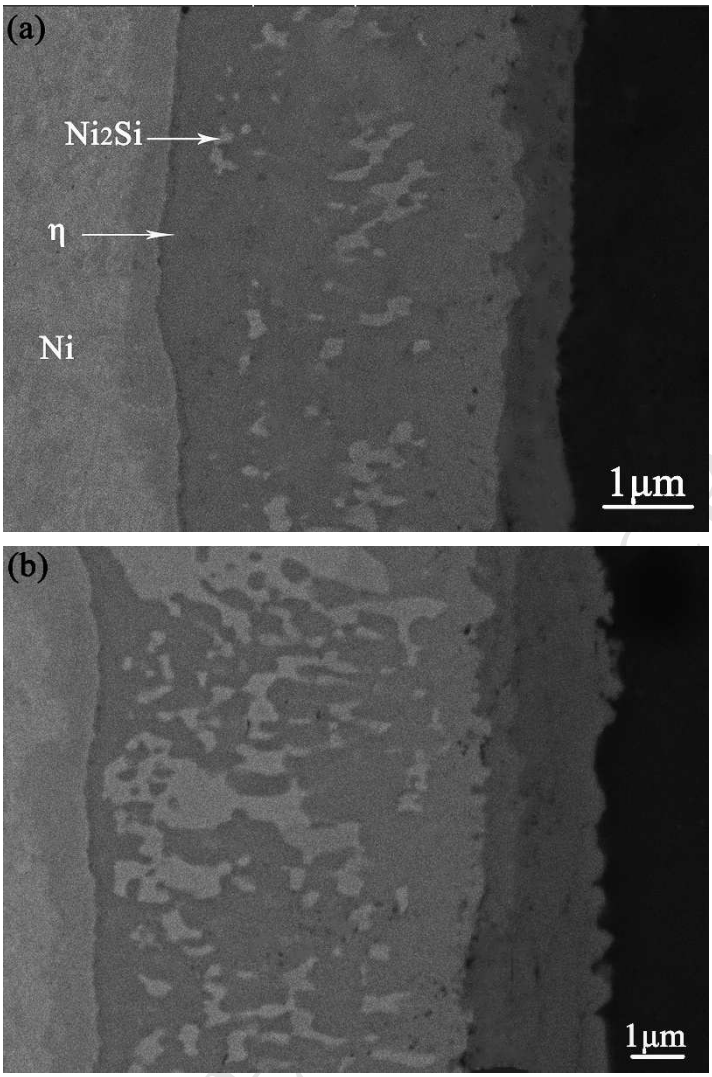

Fig. 4. Microstructure of Cu/Ni/Mg_2Si interfaces formed at 1023K with different holding times: (a) 5 min, (b) 30 min.

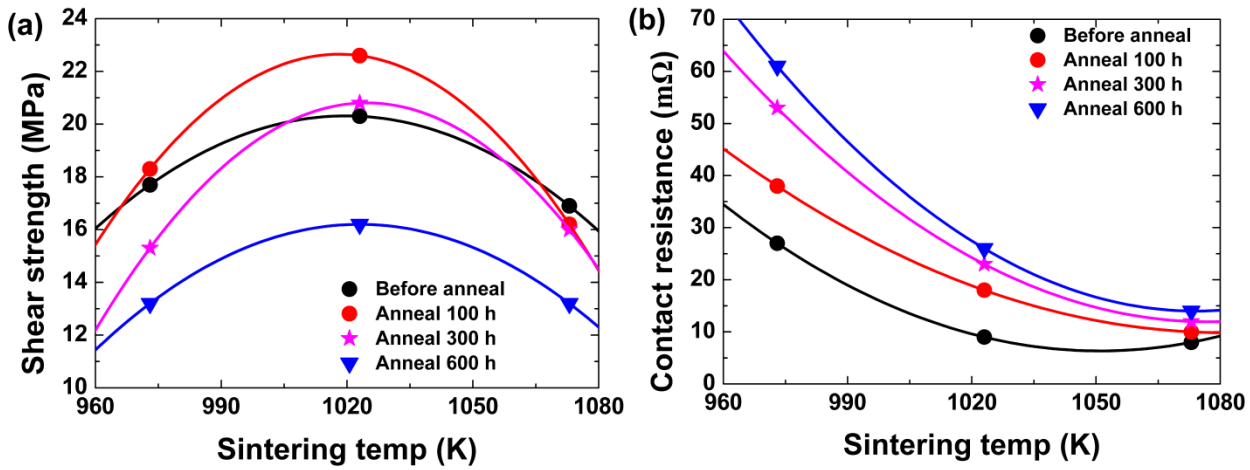

Fig. 5. Effect of annealing time at 723K on: (a) shear strength and (b) contact resistance of Cu/Ni/Mg_2Si joints sintered at different temperatures for 15 min.

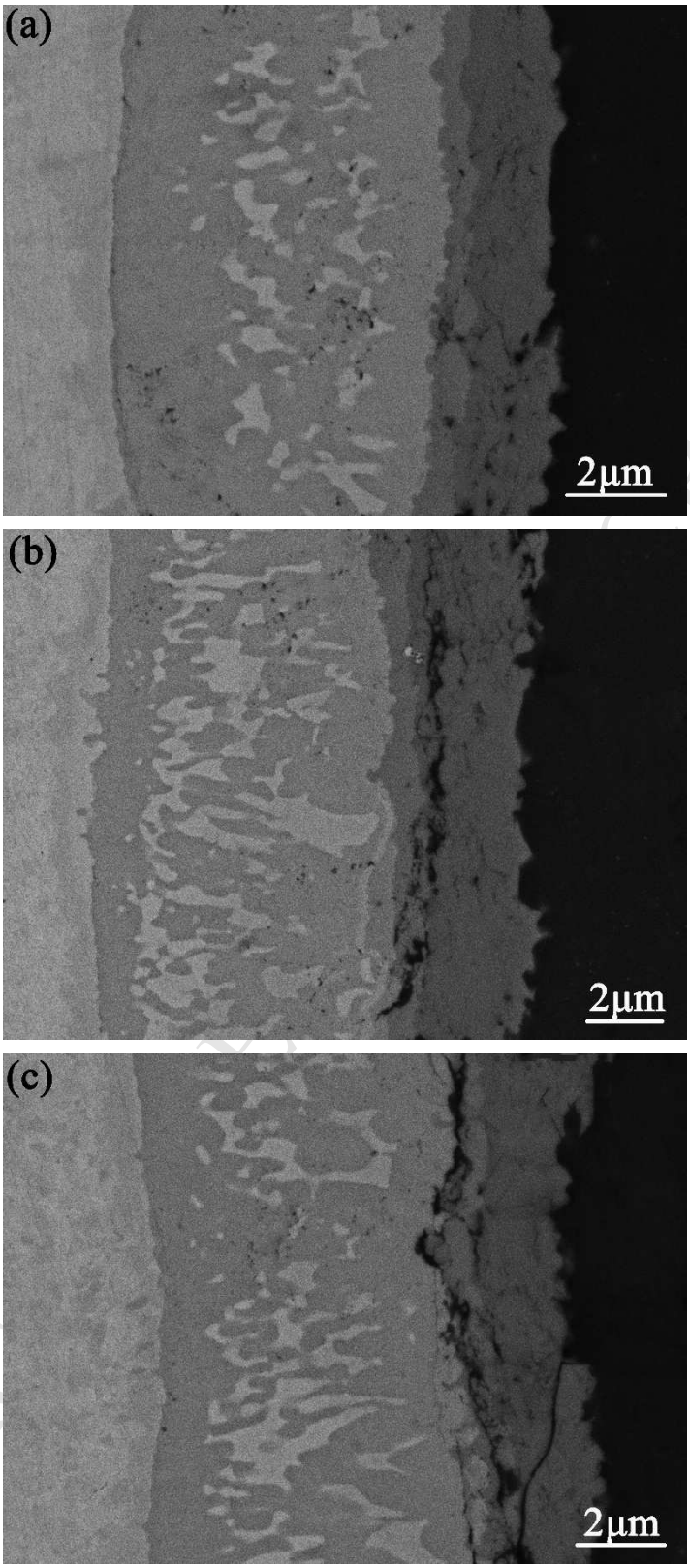

Fig. 6. Microstructure of the Cu/Ni/Mg_2Si interface sintered at 1023K after annealing at 723K for (a) 100 h, (b) 300 h, (c) 600 h.

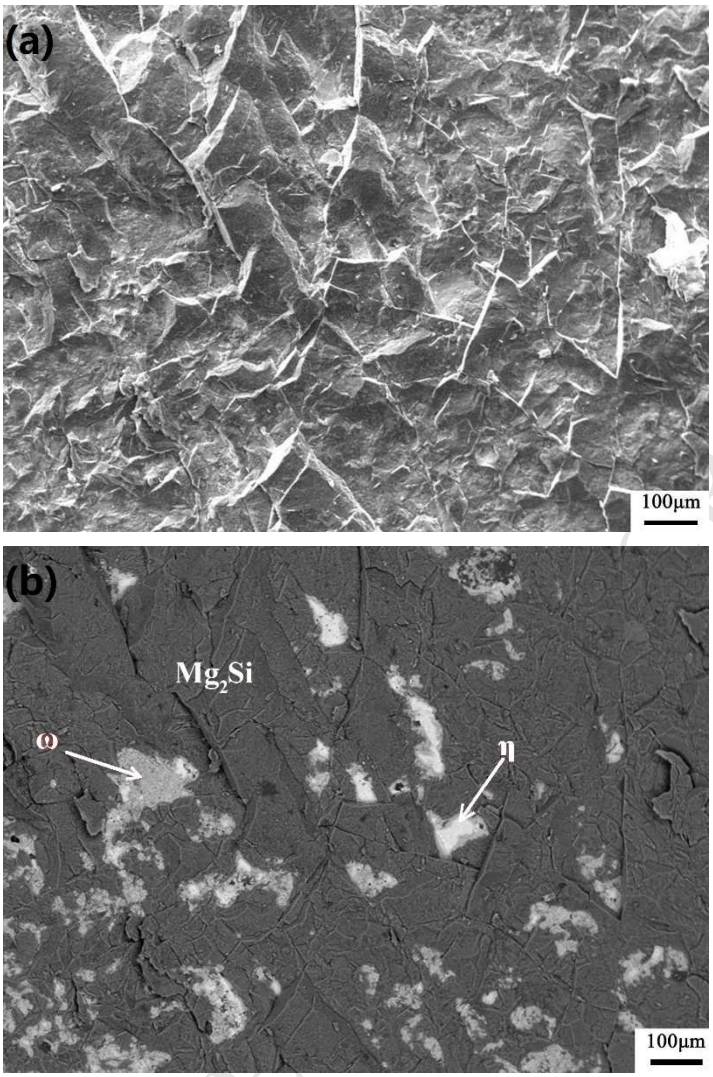

Fig. 7. (a) SEM image and (b) BSD image of a fracture surface of a sample sintered at 1023K for 30 min and annealed at 723K for 100 h.